

Higgs oscillations in time-resolved optical conductivityA. Kumar^{*} and A. F. Kemper[†]*Department of Physics, North Carolina State University, Raleigh, North Carolina 27695, USA*

(Received 19 March 2019; revised manuscript received 21 October 2019; published 21 November 2019)

Driving superconductors out of equilibrium is a promising avenue to study their equilibrium properties as well as to control the superconducting state. Nonequilibrium superconductors are often studied using time-resolved optical conductivity measurements. Thus, the characterization of a superconducting state in a pump driven nonequilibrium state requires careful attention in the time domain. We calculate the time-resolved optical conductivity of a pumped superconducting state using a nonequilibrium Keldysh approach. Through functional derivation, the optical conductivity is obtained with full vertex corrections and used to characterize the transient superconducting state. The transient optical conductivity shows the suppression of the superconducting order parameter in the time domain. The subsequent recovery of the order parameter exhibits oscillatory behavior that corresponds to the Higgs amplitude mode, and may be seen in several parts of the spectrum.

DOI: [10.1103/PhysRevB.100.174515](https://doi.org/10.1103/PhysRevB.100.174515)

Advancements of time-resolved spectroscopic techniques have enabled the measurement [1] and control [2–7] of hidden properties of ground states and low-energy excitations in correlated materials, which are not easily accessible in equilibrium. In the energy spectrum, relatively low-energy scale—terahertz and midinfrared—frequencies have a special place in such techniques because of their noninvasive nature (to suppress the heat production that may destroy the ordered state) and suitability for observation of low-energy excitations of the ground states.

Within the context of superconductivity, the excitations of superconducting condensate are of great interest. The scalar nature of the condensate restricts any coupling to the electromagnetic (EM) field in the linear regime. Moreover, when the superconducting order is perturbed by any means, the underlying U(1) symmetry breaks spontaneously and results in two oscillating bosonic modes: the massless phase, and the massive amplitude mode—the Higgs mode [8–14]. The elusive Higgs mode resides at a frequency of twice the superconducting gap (2Δ). Recently, it has been shown that the amplitude mode can be excited, and observed, by an EM field using a coexisting order, e.g., charge density wave [15], by nonlinear coupling to the EM field (generation of the third harmonic) [16,17], by time-resolved conductivity [18], or by using the presence of supercurrent [19,20].

Given that the optical conductivity is the primary probe of the Higgs mode, a proper theoretical description of the conductivity is a necessity. Numerous work has been done to calculate the conductivity (and other response functions) of correlated electrons in an equilibrium [21–24] and nonequilibrium state [10,25–28]. In a nonequilibrium state, such as induced by a pump-probe setup, a calculation of the conductivity through the Bethe-Salpeter (BS) equation, which

is necessary to capture the effects beyond the bare-bubble susceptibility, becomes computationally prohibitive because the Hamiltonian loses time-translational symmetry. Previous solutions to this problem include exact diagonalization of the Hamiltonian (which is limited by system size), mean-field analyses of the BCS Hamiltonian (which is *a priori* not gauge invariant and neglects inelastic collisions and dynamics of the interactions) [29], and the time-dependent dynamical mean-field theory (td-DMFT) [30,31] where optical conductivity of a superconductor was not considered.

In this work, we go beyond these limitations and calculate the time-dependent optical conductivity using a functional derivation approach based on nonequilibrium Green's functions. We solve the Nambu-Gor'kov equations for electron-phonon mediated superconductivity self-consistently on the Keldysh contour and calculate the nonequilibrium interacting Green's functions in the time domain. We consider the Holstein model with impurity scattering as a particular instance to study the transient optical conductivity of a superconductor. The optical conductivity is calculated by a functional derivative of the current with respect to the applied field. One of the advantages of this particular method is that it naturally includes vertex corrections [32–34], but bypasses the calculation of the BS equation in the time domain. In equilibrium, our results reproduce several features of the known conductivity of dirty superconductors such as an upturn towards low frequencies inside the gap [21,22]. In a pump driven, nonequilibrium case, the conductivity reflects the temporal dynamics of superconducting order including suppression, recovery, and the Higgs oscillations. These are clearly present in the features of the conductivity that are commonly associated with the superconducting order in equilibrium, i.e., the energy location of the gap, the coherence peak, and the phonon features in the real part of the conductivity, as well as in the inductive $1/\omega$ low-frequency response in the imaginary part. We quantify and characterize the transient superconducting state using these features as well as purely

^{*}akumar13@ncsu.edu[†]akemper@ncsu.edu

time domain feature (the probe current). All the quantities show excellent correlation to the gap dynamics which are known from the underlying simulations [12].

Methods. We consider the Holstein Hamiltonian on two-dimensional (2D) square lattice to simulate a phonon-mediated, s -wave superconductor,

$$\mathcal{H} = \sum_{\mathbf{k}, \sigma} \xi(\mathbf{k}) c_{\mathbf{k}, \sigma}^\dagger c_{\mathbf{k}, \sigma} + \Omega \sum_{\mathbf{q}} \left(b_{\mathbf{q}}^\dagger b_{\mathbf{q}} + \frac{1}{2} \right) + \frac{g}{\sqrt{N}} \sum_{\mathbf{k}, \mathbf{q}} c_{\mathbf{k}+\mathbf{q}, \sigma}^\dagger c_{\mathbf{k}, \sigma} (b_{\mathbf{q}} + b_{-\mathbf{q}}^\dagger) + \sum_{i, \sigma} V_i c_{i, \sigma}^\dagger c_{i, \sigma}. \quad (1)$$

Here, $\xi(\mathbf{k}) (= -2V_{nn}[\cos(k_x) + \cos(k_y)] - \mu)$ is the nearest-neighbor tight-binding energy dispersion measured relative to the chemical potential μ , $c_{\mathbf{k}}^\dagger, c_{\mathbf{k}}$ ($b_{\mathbf{q}}^\dagger, b_{\mathbf{q}}$) are the standard creation and annihilation operators for an electron (phonon), g is the momentum-independent e -ph coupling constant, and Ω is the frequency for the Einstein phonon. V_i is the coupling between electrons and impurities which are distributed randomly on lattice sites. The choice of the Hamiltonian is appropriate for the time-dependent problem considered here as the Hamiltonian can be handled computationally. While this model was originally developed for electron-phonon problems, a formally identical boson exchange model can be used to treat repulsive spin-fluctuation-mediated interactions [35].

The phonon subsystem is treated as a heat reservoir whose properties do not change in time as we drive the electronic subsystem, which is valid for the small pump fluences considered here [36,37]. The interactions are treated within a self-consistent diagrammatic-perturbative framework, which sums the diagrams to all orders of a subclass of diagrams (see the Supplemental Material [38]) and ensures the conservation laws [39]. The superconducting state is treated within a self-consistent Migdal-Eliashberg formalism, and the time evolution is done by solving the Gor'kov equations self-consistently on the Keldysh contour [12,38] (see also Refs. [34,40–42]).

The pump field, which is applied in the (11) direction, is included via the minimal coupling i.e., Peierls' substitution $\mathbf{k}(t) = \mathbf{k} - \mathbf{A}(t)$. In addition to the pump pulse, a secondary (probe) pulse is included in the same way as the pump. However, the probe amplitude and frequency are optimized to ensure that the probe is in the linear-response regime and is able to probe the conductivity within the 2Δ range. The pump and probe pulse envelopes are taken to be Gaussian curves $\mathbf{A}(t') = A_{\max} \sin[\omega(t' - t_0)] \exp(-\frac{(t' - t_0)^2}{2\sigma^2})(1, 1)$ with different parameters.

For the simulation, we use band electronic parameters $V_{nn} = 0.25$, $\mu = 0.0$ eV, phonons parameters $\Omega = 0.2$, $g^2 = 0.12$ eV and impurity coupling $\langle V_i \rangle^2 = 0.01$ eV. These parameters result in an equilibrium superconducting gap $\Delta \approx 46$ meV at temperature $T \approx 83$ K. The choice of parameters does not represent a specific material. Rather, the parameters were chosen for numerical tractability. For the pump and probe field we use $\omega_p = 1.5$ eV, $\sigma_p = 8$ (1/eV) and $\omega = 0.01$ eV, $\sigma = 3$ (1/eV), respectively.

To calculate transient conductivity we have used the algorithm proposed in Refs. [33,34,43]. The central idea

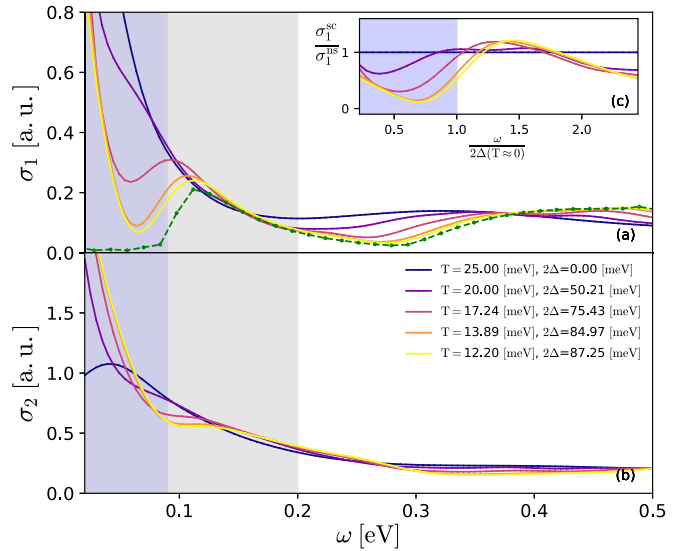


FIG. 1. The conductivity of the Holstein model in equilibrium. Panels (a) and (b) show the real and the imaginary part of optical conductivity at different temperatures, respectively. The temperature range spans the superconducting phase transition. The dark shaded region shows the maximum superconducting optical gap near zero temperature $2\Delta(T \approx 0)$. The light shaded region shows the phonon window ($0 < \omega < \Omega = 0.2$ eV). Panel (c) displays the ratio of real parts of conductivity in the superconducting state to normal state at $T = 25$ meV. The dashed line in panel (a) shows σ_1 calculated using bare-bubble susceptibility at $T = 12.2$ meV.

is that first we calculate nonequilibrium current \mathbf{J}_{pump} for the pumped state without a probe via $\mathbf{J}(t_a) = N_{\mathbf{k}}^{-1} \sum_{\mathbf{k}} \nabla \xi(\mathbf{k} - \mathbf{A}) \text{Im} G_{\mathbf{k}}^<(t', t'' = t')$, where $t_a = \frac{t'+t''}{2}$ and the derivative is taken along the field (11) direction. Then, for each pump-probe delay time ($t = \text{probe}_{\text{center}} - \text{pump}_{\text{center}}$), we calculate change in the current as function of time ($\delta \mathbf{J} = \mathbf{J}_{\text{pump+probe}} - \mathbf{J}_{\text{pump}}$). The current and the probe time profiles are then used to calculate time-dependent conductivity as $\sigma(t, \omega) = \frac{\delta \mathbf{J}(t, \omega)}{\mathbf{E}_{\text{probe}}(\omega)}$. Here, we have taken the Fourier transform along average-time axis t_a ($t' = t''$). However, depending on the experimental settings other time axes can also be used to take the Fourier transform, as described in Refs. [44–49]. For this particular choice, the length of the time signal averages out the amplitude of the Higgs mode.

Equilibrium results. First, we calculate the conductivity of the system in an equilibrium state, i.e., without a pump field. The results are shown in Fig. 1 as a function of temperature T . For reference, we have also labeled the curves by their equilibrium superconducting gap 2Δ as determined from the static component of the anomalous retarded self-energy $\Sigma_R^F(\omega = 0)$. In the normal state ($T > T_c$) we observe the Drude features in the conductivity near zero frequency, and the effect of the Einstein phonon at the phonon frequency Ω . The presence of a phonon lowers the optical spectral weight in the vicinity of the phonon frequency (Ω); this may be observed as a flattening of the spectral weight in σ_1 at Ω . It is important to note that the minimum of the real part of the conductivity lies at the phonon frequency Ω in the normal state and shifts by 2Δ in the superconducting state. This particular feature will be used

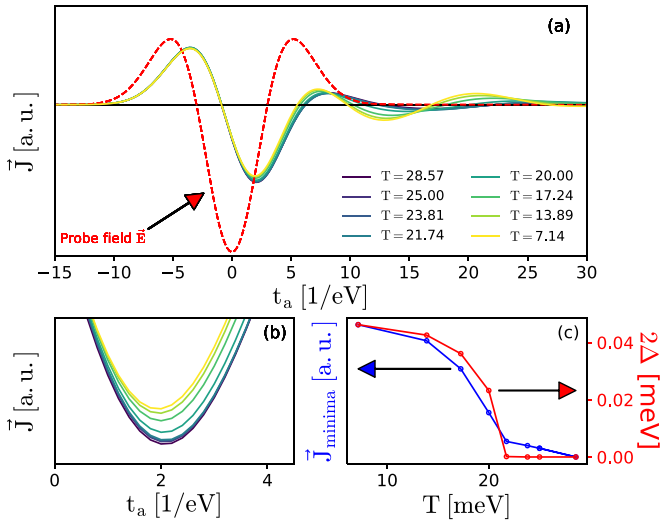


FIG. 2. Probe current in equilibrium state. Panel (a) shows the probe current as a function of time at different temperatures in equilibrium. The temperature range spans the superconducting phase transition. Panel (b) displays the zoomed region around the global minimum of the probe current. Panel (c) shows the correlation between the probe-current minimum and the superconducting order parameter calculated using $\Sigma_R^F(\omega = 0)$.

to study the dynamics of the superconducting edge (the gap) in the superconducting state.

In the superconducting state ($T < T_c$) we observe the opening of the gap in the conductivity i.e., the lowering of the optical spectral weight inside the 2Δ window (marked by the first shaded region in the figure near zero frequency). In addition, we note the shift of the minimum around the phonon frequency from Ω to $\Omega + 2\Delta$. The normalized conductivity $[\sigma_1(T < T_c)/\sigma_1(T = 25)]$ is plotted in inset (c), which clearly shows the opening of the gap and the development of the coherence peak. The imaginary part of the conductivity [Fig. 1(b)] can also be analyzed in a similar way to characterize the superconducting state; it shows $\frac{1}{\omega}$ behavior inside the 2Δ window. For comparison we include the conductivity calculated from the bare-bubble susceptibility $\chi(\mathbf{q} = 0, \omega) = \int d(t' - t'') \sum_{\mathbf{k}} |\mathbf{v}_{\mathbf{k}}|^2 [G_{\mathbf{k}}^>(t', t'') G_{\mathbf{k}}^<(t'', t') - G_{\mathbf{k}}^<(t', t'') G_{\mathbf{k}}^>(t'', t')] e^{-i\omega(t' - t'')}$ in the figure (dashed line). We observe noticeable qualitative differences because of the vertex corrections in the conductivity calculated from the functional derivation of probe current, mainly near the gap edge and for low energies.

As has been shown in THz pump-probe experiments [18], the probe current maximum or minimum can also be used as an indicator to study changes in the physical state of a system, e.g., phase transitions or pump induced changes in the system response. We analyze our data in a similar way and plot the equilibrium probe current at different temperatures ranging from normal state to the superconducting state in Fig. 2. As the temperature is reduced, rapid oscillations appear in the probe current, and the minimum is reduced [see Fig. 2(b)]. The minimum of the probe current directly correlates with the superconducting order parameter, which is shown in panel (c) where we plot the first minimum of the probe current and the superconducting order parameter. This particular feature

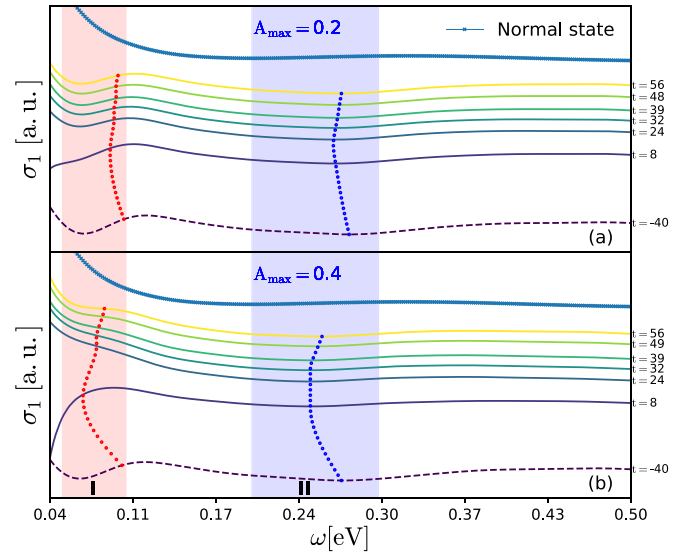


FIG. 3. Conductivity of the system in a pump driven nonequilibrium state. Panels (a) and (b) show the real part of optical conductivity as a function of frequency at different delay times for pump fluence $A_{\text{max}} = 0.2$ ($1/a_0$) and 0.4 ($1/a_0$). Each curve is shifted by an offset (scaled as the delay time) along Y axis to show the changes in the transient conductivity. The top dashed line in each panel shows the conductivity of normal state in equilibrium. Conductivity of the superconducting state is shown by $t = -40$ (1/eV) in equilibrium. The blue shaded region II shows the vicinity where the location of the σ_1 minimum resides near the phonon frequency Ω . The minima are shown by the dotted curve connecting different delay-time curves. The red shaded region I shows the region where the gap edge is located and marked by the dotted line connecting different delay-time curves.

can also be used to characterize the transient conductivity in a pump driven superconductor which is shown in the following sections.

Pump-probe results. Next, we discuss the dynamics of electrons in a pump-driven nonequilibrium state. Figure 3 shows the real part (σ_1) of the transient conductivity as a function of pump-probe delay time for two pump fluences $A_{\text{max}} = 0.2, 0.4$ ($1/a_0$). We observe noticeable changes in the conductivity from the equilibrium state [at $t = -40$ (1/eV)]. Mainly, the suppression of superconducting order can be observed as the edge of the gap (indicated by red markers in region I) moving towards zero during early delay times. The second indicator, the location of the minimum in the real part of the conductivity near the phonon frequency Ω , also shifts on the frequency axis. These minima are located within the shaded region II in the figure. Such suppression of superconductivity is expected in the transient state of the system when the pump drives the system because, intuitively, the pump injects energy in the system and creates excitations. These excitations raise the effective temperature of the system and result in the observed superconducting order suppression. It is important to notice that the effective-temperature picture does not imply a local equilibrium in the transient state as shown previously [12,13,50]. Rather, the system is in a dynamic nonthermal state where oscillation of the superfluid condensate is observed (this will be discussed in the following

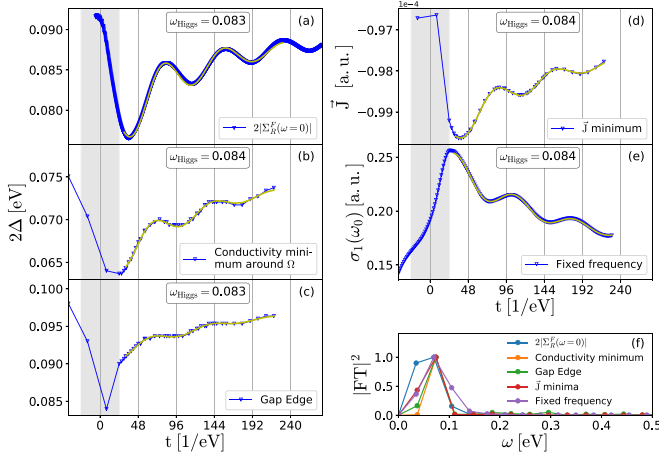


FIG. 4. Higgs oscillation. The figure shows the dynamics of the superconducting order parameter in a pump induced nonequilibrium state [for $A_{\max} = 0.2$ ($1/a_0$)]. Panel (a) shows the order parameter as a function of average time calculated using anomalous self-energy. Panels (b) and (c) display the estimated order parameter using the location of the minimum of the real part of optical conductivity around the phonon frequency (shown in the blue shaded region II in Fig. 3) and the gap edge location (the red shaded region I in Fig. 3), respectively. Panels (d) and (e) show the probe current minimum and $\sigma_1(\omega = 0.09)$ as a function of time, respectively. All five quantities shown in panels exhibit oscillations in time with approximately same frequency [$\omega_{\text{Higgs}} \approx 2\Delta(t)$], which is calculated by fitting the data to an oscillatory decaying function. The Fourier transform of the data also shows a peak at the same frequency (f).

sections). For the larger fluence $A_{\max} = 0.4$ ($1/a_0$), the melting of the superconducting order is stronger and the gap is closed further. Furthermore, it is important to notice that for larger fluences the conductivity (σ_1) does not show a “clear” spectral gap in the spectrum as shown in Fig. 3(b) at delay time $t = 24$ ($1/\text{eV}$). However, the superconductivity remains in the system (as evidenced by a finite off-diagonal order) as shown here [12]. Out of equilibrium, the direct connection between a gap in the optical spectra and finite off-diagonal order is broken.

Here, we study the dynamics of the superconducting order parameter in the pump-induced nonequilibrium state from the perspective of the time-resolved optical conductivity. Mainly, we discuss the presence of the Higgs mode in our simulation. Here they arise from a time dependence of the underlying order parameter, which is reflected in the time-dependent conductivity. For reference, we will use the superconducting gap $\Delta = \Sigma_K^R(\omega = 0)$ as a function of average time. We may estimate the order parameter using the gap edge in $\sigma_1(\omega)$, which in equilibrium occurs at $\omega = 2\Delta$. We define the edge of the gap as the point ω_{edge} on the frequency axis where the mean of $(\frac{\sigma_1^{\text{sc}}}{\sigma_1^{\text{ns}}})_{\text{max}}$ and $(\frac{\sigma_1^{\text{sc}}}{\sigma_1^{\text{ns}}})_{\text{min}}$ is located within the shaded region I in Fig. 3. Similarly, we use the $\sigma_1(\omega)$ minimum around the phonon frequency Ω as a reference. These markers are shown in Figs. 4(a)–4(c), respectively. We observe that the order parameter determined from Σ_K^R is suppressed when the pump is active at early times, and

it recovers back to the equilibrium value for later times, exhibiting Higgs oscillations as it recovers. The gap edge and the minimum location exhibit similar behavior, although the relative change is larger at the minimum. All three quantities show Higgs oscillations at approximately the same frequency—in principle the frequency is time dependent as it scales with the local (in time) gap [12], however in this time range is it approximately constant. Note that there is a small discrepancy in the order parameter value calculated using various pieces of the conductivity data which may arise due to the particular choice of delay axis to Fourier transform, and due to the frequency resolution of the probe signal.

Besides these markers, the Higgs oscillations occur across the response. For example, the probe-current minimum as a function of delay time shows the Higgs oscillations as well [cf. Fig. 4(d)]. Finally, the oscillatory behavior can also be observed when considering σ_1 at some fixed frequency ω_0 as shown in Fig. 4(e). Here we have chosen ω_0 within the 2Δ window, but the oscillation of the conductivity may be seen at all frequencies as a function of time delay [Fig. 4(c)] [38].

Figure 4(f) presents the Fourier transform of the quantities shown in Figs. 4(a)–4(e). Although the limited data length leads to wide peaks, the various measurements all oscillate at the same frequency. This is further confirmed by a curve fit to a decaying oscillation (shown on the individual panels), which yields the same frequency for all the measures.

In summary, we have presented the time-resolved optical conductivity of a pumped superconductor based on the gauge invariant, fully vertex corrected method. The results show that the entire spectrum undergoes changes that reflect the underlying changes in the gap. There are shifts (in energy) of features in the conductivity due to the reduction from $\Delta_{\text{equilibrium}}$ to some reduced $\Delta(t)$, which itself oscillates in time. These “Higgs” oscillations are thus visible in essentially the entire spectrum. We quantify several features that are known to correspond to the gap in equilibrium, e.g., the gap edge and the phonon minimum, and connect them to the underlying gap dynamics which are known from the calculations.

We stress the suitability of the method used in this work to calculate transient optical conductivity. The method enables calculation of the response functions beyond the bare-bubble susceptibility. The effect of vertex corrections varies depending on the particulars of the system. For example, they are expected to be minor for an electron-phonon system in the Migdal limit, but not negligible when it comes to impurity scattering in certain regimes (this effect is observed in Fig. 1 for low energies where the impurity scattering is significant). The functional derivative method captures these faithfully and may have broader applicability in the evaluation of equilibrium and nonequilibrium two-particle quantities.

ACKNOWLEDGMENTS

We acknowledge fruitful discussion with A. Rustagi. This work was partly supported by NSF Grant No. DMR-1752713. This research used resources of the National Energy Research Scientific Computing Center, a DOE Office of Science User Facility supported by the Office of Science of the U.S. Department of Energy under Contract No. DE-AC02-05CH11231.

- [1] J. Graf, C. Jozwiak, C. L. Smallwood, H. Eisaki, R. A. Kaindl, D.-H. Lee, and A. Lanzara, *Nat. Phys.* **7**, 805 (2011).
- [2] D. Fausti, R. I. Tobey, N. Dean, S. Kaiser, A. Dienst, M. C. Hoffmann, S. Pyon, T. Takayama, H. Takagi, and A. Cavalleri, *Science* **331**, 189 (2011).
- [3] W. Hu, S. Kaiser, D. Nicoletti, C. R. Hunt, I. Gierz, M. C. Hoffmann, M. L. Tacon, T. Loew, B. Keimer, and A. Cavalleri, *Nat. Mater.* **13**, 705 (2014).
- [4] M. Mitrano, A. Cantaluppi, D. Nicoletti, S. Kaiser, A. Perucchi, S. Lupi, P. Di Pietro, D. Pontiroli, M. Riccò, S. R. Clark, D. Jaksch, and A. Cavalleri, *Nature (London)* **530**, 461 (2016).
- [5] X. Yang, C. Vaswani, C. Sundahl, M. Mootz, P. Gagel, L. Luo, J. H. Kang, P. P. Orth, I. E. Perakis, C. B. Eom, and J. Wang, *Nat. Mater.* **17**, 586 (2018).
- [6] X. Yang, L. Luo, M. Mootz, A. Patz, S. L. Bud'ko, P. C. Canfield, I. E. Perakis, and J. Wang, *Phys. Rev. Lett.* **121**, 267001 (2018).
- [7] X. Yang, X. Zhao, C. Vaswani, C. Sundahl, B. Song, Y. Yao, D. Cheng, Z. Liu, P. P. Orth, M. Mootz, J. H. Kang, I. E. Perakis, C.-Z. Wang, K.-M. Ho, C. B. Eom, and J. Wang, *Phys. Rev. B* **99**, 094504 (2019).
- [8] A. F. Volkov and S. M. Kogan, *Sov. J. Exp. Theor. Phys.* **38**, 1018 (1974).
- [9] P. B. Littlewood and C. M. Varma, *Phys. Rev. B* **26**, 4883 (1982).
- [10] H. Krull, D. Manske, G. S. Uhrig, and A. P. Schnyder, *Phys. Rev. B* **90**, 014515 (2014).
- [11] T. Cea, C. Castellani, G. Seibold, and L. Benfatto, *Phys. Rev. Lett.* **115**, 157002 (2015).
- [12] A. F. Kemper, M. A. Sentef, B. Moritz, J. K. Freericks, and T. P. Devereaux, *Phys. Rev. B* **92**, 224517 (2015).
- [13] A. Kumar, S. Johnston, and A. F. Kemper, *Europhys. Lett.* **124**, 67002 (2019).
- [14] Y. Murakami, P. Werner, N. Tsuji, and H. Aoki, *Phys. Rev. B* **93**, 094509 (2016).
- [15] M.-A. Méasson, Y. Gallais, M. Cazayous, B. Clair, P. Rodière, L. Cario, and A. Sacuto, *Phys. Rev. B* **89**, 060503(R) (2014).
- [16] R. Matsunaga, N. Tsuji, H. Fujita, A. Sugioka, K. Makise, Y. Uzawa, H. Terai, Z. Wang, H. Aoki, and R. Shimano, *Science* **345**, 1145 (2014).
- [17] K. Katsumi, N. Tsuji, Y. I. Hamada, R. Matsunaga, J. Schneeloch, R. D. Zhong, G. D. Gu, H. Aoki, Y. Gallais, and R. Shimano, *Phys. Rev. Lett.* **120**, 117001 (2018).
- [18] R. Matsunaga, Y. I. Hamada, K. Makise, Y. Uzawa, H. Terai, Z. Wang, and R. Shimano, *Phys. Rev. Lett.* **111**, 057002 (2013).
- [19] S. Nakamura, Y. Iida, Y. Murotani, R. Matsunaga, H. Terai, and R. Shimano, *Phys. Rev. Lett.* **122**, 257001 (2019).
- [20] A. Moor, A. F. Volkov, and K. B. Efetov, *Phys. Rev. Lett.* **118**, 047001 (2017).
- [21] D. C. Mattis and J. Bardeen, *Phys. Rev.* **111**, 412 (1958).
- [22] W. Zimmermann, E. H. Brandt, M. Bauer, E. Seider, and L. Genzel, *Phys. C (Amsterdam, Neth.)* **183**, 99 (1991).
- [23] H. Chen, *Phys. Rev. Lett.* **71**, 2304 (1993).
- [24] A. V. Chubukov and D. L. Maslov, *Phys. Rev. B* **96**, 205136 (2017).
- [25] M. Eckstein and M. Kollar, *Phys. Rev. B* **78**, 205119 (2008).
- [26] M. Eckstein, M. Kollar, and P. Werner, *Phys. Rev. B* **81**, 115131 (2010).
- [27] J. Orenstein and J. S. Dodge, *Phys. Rev. B* **92**, 134507 (2015).
- [28] D. M. Kennes, E. Y. Wilner, D. R. Reichman, and A. J. Millis, *Phys. Rev. B* **96**, 054506 (2017).
- [29] Y. Nambu, *Phys. Rev.* **117**, 648 (1960).
- [30] N. Tsuji, T. Oka, and H. Aoki, *Phys. Rev. Lett.* **103**, 047403 (2009).
- [31] N. Tsuji, Y. Murakami, and H. Aoki, *Phys. Rev. B* **94**, 224519 (2016).
- [32] N. Säkkinen, M. Manninen, and R. v. Leeuwen, *New J. Phys.* **14**, 013032 (2012).
- [33] N.-H. Kwong and M. Bonitz, *Phys. Rev. Lett.* **84**, 1768 (2000).
- [34] G. Stefanucci, *Nonequilibrium Many-Body Theory of Quantum Systems: A Modern Introduction* (Cambridge University Press, Cambridge, UK, 2013).
- [35] J. P. Carbotte, T. Timusk, and J. Hwang, *Rep. Prog. Phys.* **74**, 066501 (2011).
- [36] O. Abdurazakov, D. Nevola, A. Rustagi, J. K. Freericks, D. B. Dougherty, and A. F. Kemper, *Phys. Rev. B* **98**, 245110 (2018).
- [37] Y. Murakami, P. Werner, N. Tsuji, and H. Aoki, *Phys. Rev. B* **91**, 045128 (2015).
- [38] See Supplemental Material at <http://link.aps.org/supplemental/10.1103/PhysRevB.100.174515> for additional details of the method and the used approximations. A movie of the time-resolved conductivity is also included.
- [39] G. Baym and L. P. Kadanoff, *Phys. Rev.* **124**, 287 (1961).
- [40] A. Stan, N. E. Dahlen, and R. van Leeuwen, *J. Chem. Phys.* **130**, 224101 (2009).
- [41] H. Bruus, *Many-Body Quantum Theory in Condensed Matter Physics: An Introduction* (Oxford University Press, Oxford, 2004).
- [42] G. Mahan, *Many-Particle Physics* (Kluwer/Plenum, New York, 2000).
- [43] C. Shao, T. Tohyama, H.-G. Luo, and H. Lu, *Phys. Rev. B* **93**, 195144 (2016).
- [44] C. H. B. Cruz, J. P. Gordon, P. C. Becker, R. L. Fork, and C. V. Shank, *IEEE J. Quantum Electron.* **24**, 261 (1988).
- [45] P. Hamm, *Chem. Phys.* **200**, 415 (1995).
- [46] J. T. Kindt and C. A. Schmuttenmaer, *J. Chem. Phys.* **110**, 8589 (1999).
- [47] H. Němec, F. Kadlec, and P. Kužel, *J. Chem. Phys.* **117**, 8454 (2002).
- [48] R. D. Averitt and A. J. Taylor, *J. Phys.: Condens. Matter* **14**, R1357 (2002).
- [49] H.-K. Nienhuys and V. Sundström, *Phys. Rev. B* **71**, 235110 (2005).
- [50] B. Nosarzewski, B. Moritz, J. K. Freericks, A. F. Kemper, and T. P. Devereaux, *Phys. Rev. B* **96**, 184518 (2017).